Multi-fidelity Surrogate-integrated Modelling Framework: Application to Tall Energy Structures

Wuhua Xie[1] Ke Ke[1, *] Guohao Wang[3] and Honghu Chu[2, 3]

[1]School of Civil Engineering, Chongqing University, China
[2]College of Civil Engineering and Architecture, Zhejiang University of Water Resources and Electric Power, China
[3]Bartlett School of Sustainable Construction, University College London, United Kingdom
wuhuaxie1995@gmail.com, ke.ke@cqu.edu.cn, ucbvanb@ucl.ac.uk, chuhh@zjweu.edu.cn

Abstract –

Tall renewable energy infrastructures are complex structural systems comprising numerous components. Under earthquakes, their designated energy-dissipating components may exhibit intricate material and geometric nonlinearities that require high-fidelity finite element (FE) modelling, whereas system-level seismic assessment typically demands extensive nonlinear time-history analyses, making uniformly refined modelling computationally prohibitive. This paper presents a multi-fidelity surrogate-integrated modelling framework that concentrates refined FE simulations on the critical component to construct a surrogate model, which is then integrated into an efficient system-level model with simplified representations for the remaining components. The surrogate was developed using a multilayer perceptron (MLP) trained to jointly predict a vector of hysteretic parameters, enabling shared representation learning to capture inter-parameter correlations and thereby improving predictive accuracy and output consistency. The framework was demonstrated on a representative 10-MW resilient jacket-type offshore wind turbine, in which an hourglass-like stiffened tower segment was characterised using a comprehensive hysteresis database – derived from 3,000 refined FE simulations – and integrated into an OpenSees-based system model. The results show that the joint-prediction MLP achieved higher predictive accuracy than independently trained single-output models, while enabling efficient large-scale nonlinear dynamic analyses.

Keywords –

Energy infrastructures; seismic assessment; surrogate; multi-fidelity modelling; hysteretic behaviour

1 Introduction

Over the past decade, renewable energy has expanded rapidly worldwide, driving the deployment of tall energy infrastructures such as wind turbine towers [1] and concentrated solar power towers [2]. The expansion of these installations into seismically active regions poses significant seismic risks to the infrastructures, owing to their highly slender and cantilever-dominated structural characteristics [3]. Such slender systems can be particularly sensitive to dynamic excitations, making it challenging to sustain functionality and structural integrity under seismic hazard demands [4].

To enhance the structural performance of tall energy infrastructures, several novel structural systems equipped with energy dissipation devices, such as tuned mass dampers [5, 6], tuned liquid dampers [7, 8], and ductile tower segments [9, 10], have been developed. Their seismic performance assessment is particularly challenging because it often requires extensive nonlinear time-history analyses (NLTHAs) to capture seismic response, damage evolution, and failure modes. However, modelling such systems inevitably involves a trade-off between computational accuracy and efficiency [11]. Applying uniformly high-fidelity modelling to the entire structural system becomes prohibitive when hundreds or thousands of NLTHAs are required for record-to-record variability or parametric studies [12]. For example, a prior study on the 10-MW jacket-type offshore wind turbine (JOWT) reported that a refined finite element (FE) model required 36 hours to compute a single case on a 24-core workstation, even without accounting for material nonlinearity [13]. In contrast, simplified beam-based models offer efficiency but may inadequately represent the critical components that exhibit strong geometric and material nonlinearities.

Recent advances in machine learning (ML) have provided a promising solution to address this trade-off by developing data-driven surrogate models that emulate high-fidelity nonlinear behaviour at a fraction of the computational cost [14-18]. This paper proposes a multi-fidelity surrogate-integrated modelling framework to facilitate the seismic performance assessment of tall energy infrastructures. The key idea is to concentrate refined FE simulations on the critical component that dominates nonlinear deformation and energy dissipation, to construct a hysteresis database, and to train a surrogate model that maps structural design variables to a hysteretic representation. The trained surrogate model is then integrated into an efficient system-level model in which the remaining components are represented using computationally cheaper beam elements, without compromising the macroscopic fidelity of the nonlinear structural behaviour. This framework is demonstrated using a representative tall energy structure (a 10-MW resilient JOWT), where an hourglass-like stiffened tower segment (HSTS) is characterised using a hysteresis database derived from 3,000 refined FE simulations and integrated into an OpenSees system model.

A further emphasis of this study concerns the surrogate formulation. Instead of training multiple independent single-output regressors [15-18], this study adopts a single multilayer perceptron (MLP) trained to jointly predict a vector of hysteretic parameters. Multiple independently trained single-output models may yield outputs that are mutually incompatible and can violate the physical constraints implied by the actual structural behaviour. In contrast, the multi-output MLP leverages shared latent representations, allowing the model to learn cross-parameter dependencies, inherently constraining its outputs to a jointly feasible region, thereby promoting physical consistency among the outputs.

2 Methodology

This study develops a multi-fidelity surrogate-integrated modelling framework that combines refined FE simulations with data-driven surrogate modelling and an efficient system-level model. The framework targets the critical component (or component group) that dominates nonlinear deformation and energy dissipation, to which the accuracy of structural behaviour prediction is highly sensitive, while representing the remaining components using computationally cheaper modelling techniques suitable for system-level dynamics. Figure 1 shows the stepwise workflow of the proposed framework:

(1) Parameterised high-fidelity modelling of the critical component. A refined FE model is formulated and parameterised to support automated generation of component variants over a prescribed design space.

(2) Design-space sampling and database generation. A structural parameter matrix is constructed to span the practical design space, and cyclic/monotonic analyses are conducted on refined FE models to generate a hysteresis database representing the hysteretic behaviour.

(3) Hysteresis parameterisation. The simulated hysteretic curves are mapped to a phenomenological parameter set (e.g., stiffness, strength, ductility, hardening, and deterioration parameters) through calibration, yielding paired datasets of structural and hysteretic parameters.

(4) Surrogate model training with joint prediction. An MLP is trained to infer the hysteretic-parameter vector directly from the structural parameters by learning a shared latent representation and predicting all hysteretic parameters jointly.

(5) Reduced-order representation and system-level integration. The trained surrogate is assigned to a parameterised reduced-order representation of the critical component (e.g., concentrated plasticity formulation), which is then integrated into an efficient system-level model. All other components are modelled using simplified yet reliable elements that preserve global dynamics and essential interaction effects.

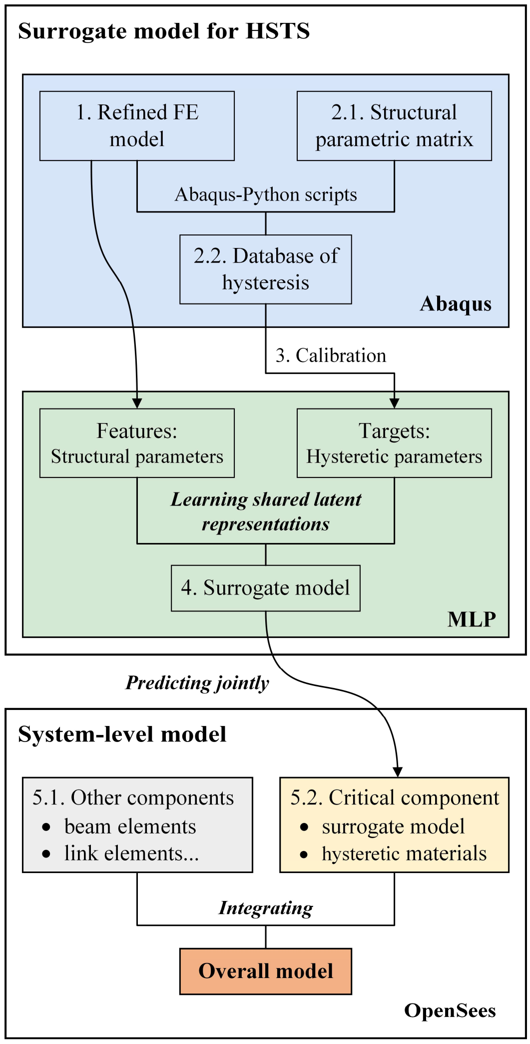

Figure 1. Multi-fidelity surrogate-integrated modelling framework

This multi-fidelity integration inevitably trades local micro-scale detail for system-level tractability. Nevertheless, by concentrating high-fidelity effort on the critical nonlinear component and ensuring that its macroscopic hysteretic behaviour is accurately reproduced via a joint-prediction surrogate, the framework provides an effective balance between fidelity and efficiency for seismic performance assessment of tall energy infrastructures.

3 Framework implementation on a 10-MW resilient JOWT

3.1 Reference structure

The multi-fidelity surrogate-integrated modelling framework is demonstrated using a representative 10-MW resilient JOWT proposed by Xie et al. [18]. This novel structural system introduces a HSTS – as the energy dissipation device – in lieu of the conventional cylindrical tower segment connecting the upper tower and transition piece of JOWTs. The HSTS is a novel component featuring complex thin-walled and stiffened configurations and necessitates a refined FE analysis to capture its initial imperfections, intricate material and geometric nonlinearities. In the following, a surrogate model is established for the HSTS and subsequently integrated into the system-level model, with the remaining components, such as the tower, rotor-nacelle assembly, and jacket foundation, modelled using computationally cheaper elements.

3.2 Automated FE modelling and hysteresis dataset generation

The refined FE models of the HSTS were established using Abaqus. Figure 2 provides further details regarding the basic geometry and structural parameters of the HSTS. This model adopted a simplified piecewise-linear material model, which is characterised by the following: (1) an elastic modulus of 210 GPa, (2) a yield stress of 355 MPa, and (3) a 1% kinematic linear strain hardening up to an ultimate stress of 470 MPa. Furthermore, the first-order 4-noded doubly curved rectangle (S4R) element was used.

Next, a comprehensive hysteresis database was generated. The database contains 3000 moment-rotation (*M-θ*) hysteretic curves obtained from refined FE simulations, covering a broad range of feasible HSTS design configurations. A structural parameter matrix was first constructed by Latin hypercube sampling within prescribed ranges selected to remain consistent with relevant design standards for stiffened-shell components. A set of Abaqus-Python scripts was then developed to enable automated processing, including:

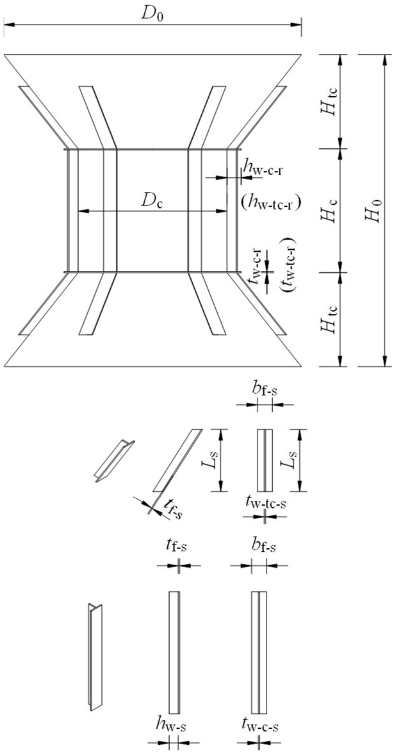

	Symbol	Description	Value range for the design space
Shells	D_0	Diameter of the original tower segment	7465 (mm)
	H_0	Height of the original tower segment	8000 (mm)
	D_c	Reduced diameter	3000~5200 (mm)
	H_c	Height of the cylindrical shell	2400~4000 (mm)
	t_c	Thickness of the cylindrical shell	28~40 (mm)
	t_{tc}	Thickness of the truncated conical shells	28~40 (mm)
	H_{tc}	Height of the truncated conical shells	$(H_0 - H_c) / 2$ (mm)
Longitudinal stiffeners	N_s	Number of stiffeners	4, 5, 6, 7, 8
	$h_{w\text{-}s}$	Width of the web	150~300 (mm)
	$t_{w\text{-}c\text{-}s}$	Thickness of the web at the middle	20~40 (mm)
	$t_{w\text{-}tc\text{-}s}$	Thickness of the web at the two ends	10~40 (mm)
	$b_{f\text{-}s}$	Width of the flange	100~200 (mm)
	$t_{f\text{-}s}$	Thickness of the flange	10~40 (mm)
	L_s	Height of the stiffener at the two ends	$(1/3 \sim 2/3) \times H_{tc}$ (mm)
Ring stiffeners	$t_{w\text{-}c\text{-}r}$	Thickness of the web at the middle	20~40 (mm)
	$h_{w\text{-}tc\text{-}r}$	Width of the web at the two ends	150~300 (mm)
	$t_{w\text{-}tc\text{-}r}$	Thickness of the web at the two ends	20~40 (mm)
	$h_{w\text{-}c\text{-}r}$	Width of the web at the middle	$h_{w\text{-}s} + 100$ (mm)

Figure 2. Basic geometry and structural parameters of the HSTS

(1) automatic generation of parameterised HSTS FE models for all sampled designs; (2) FE analyses under monotonic and cyclic loading histories consistent with FEMA 461 standard component-testing protocols; (3) post-processing of simulation results to extract the M-θ hysteretic curves; and (4) calibration of each hysteretic curve to a phenomenological representation using the modified Ibarra-Medina-Krawinkler (mIMK) model [19] parameters (Figure 3), including K_e, θ_p, θ_{pc}, M_y, M_c, and Λ.

Figure 4 summarises the calibrated mIMK parameters with their maximum, mean, minimum, and standard deviation (SD) values. Figure 5 presents representative hysteretic curves, comparing the simulations with their mIMK calibrations. The results demonstrate a high degree of accuracy.

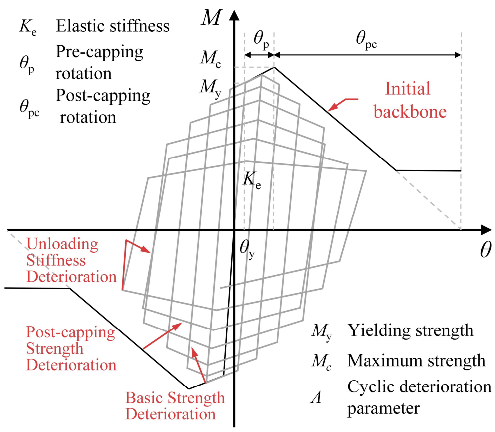

Figure 3. Illustration of the mIMK model

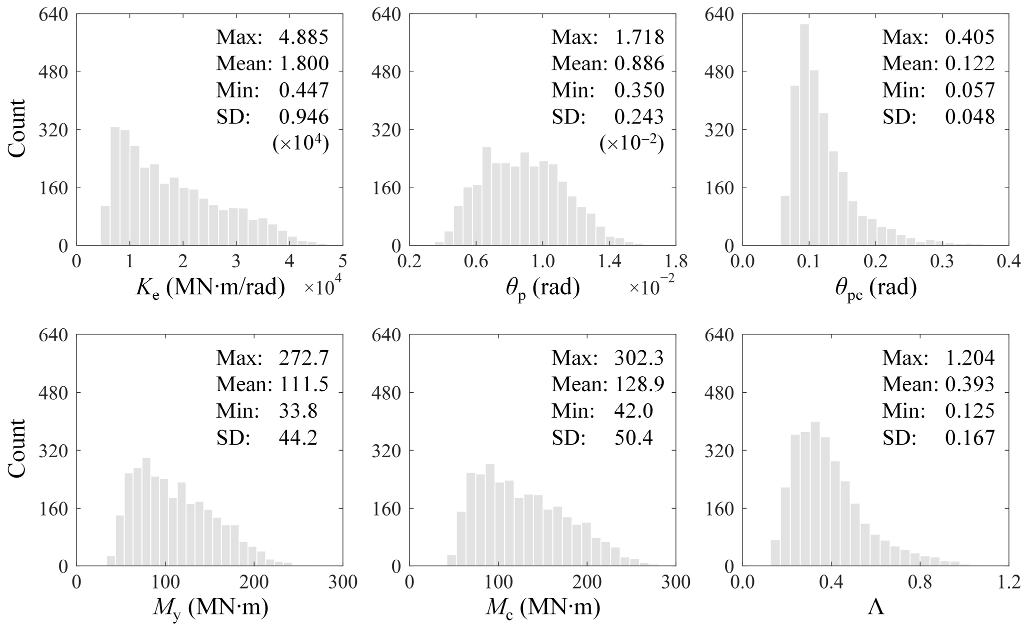

Figure 4. Calibrated mIMK parameters with the maximum, mean, minimum, and standard deviation (SD) values

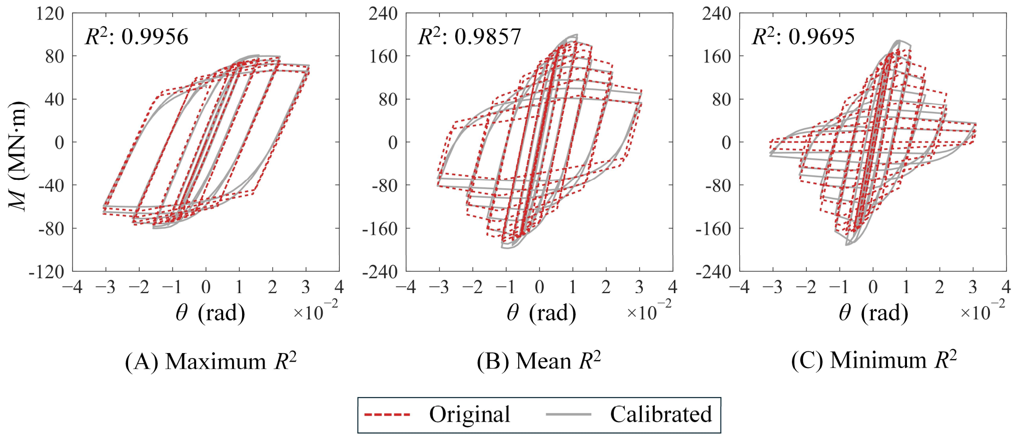

Figure 5. Representative results of hysteresis calibration

3.3 MLP surrogate model

An MLP is a feedforward neural network that learns a nonlinear mapping from input features to output targets through fully connected layers. In this study, the surrogate model is formulated as a single MLP with a vector-valued output, enabling the joint prediction of a vector of hysteretic parameters. The MLP model utilised the ReLU activation function and was trained using the Adam optimiser. The objective was to minimise the mean squared error (MSE) loss function. Training was terminated if the validation score did not improve by more than 10^{-4} for 50 consecutive iterations.

The dataset was first split into an 80/20 train/test partition (test set used only for the final evaluation). Within the training set, Optuna-based hyperparameter tuning used 5-fold cross-validation. For each fold, both inputs and outputs were standardised, and fitted on the fold training subset only to avoid data leakage. Table 1 summarises the hyperparameter search space for Optuna.

Table 1. MLP hyperparameter search space

Hyperparameter	Search space	Best
Number of hidden layers	[1, 3]	2
Units in layer i	[32, 320]	314/100
L2 regularisation	[10^{-3}, 5×10^{-2}]	0.03634
Batch size	{32, 64, 128, 256}	32
Initial learning rate	[10^{-3}, 5×10^{-3}]	0.00386

The Optuna objective maximised the mean cross-validated weighted coefficient of determination (R^2), computed as a weighted sum of per-output R^2 values. The weights for [K_e, θ_p, θ_{pc}, M_y, M_c, Λ] were set to [0.10, 0.25, 0.20, 0.10, 0.10, 0.25], following preliminary trials that indicated comparatively lower fit quality for θ_p, θ_{pc}, and Λ. The best hyperparameters were selected based on the cross-validated weighted R^2. Next, the final MLP model was trained on the full training set using the selected hyperparameters. Prediction performance was then reported on the held-out test set using per-output R^2.

Figure 6 demonstrates a good agreement between the predicted and calibrated data, confirming high performance. Table 2 further compares the R^2 and mean absolute percentage error (MAPE) achieved by the MLP model with those reported in a prior study [18] using six independently trained XGBoost models, demonstrating consistently higher accuracy for the MLP model – most notably for θ_p, θ_{pc}, and Λ.

Table 2. Prediction performance of the MLP model

Targets	MLP R^2	XGBoost R^2 [18]	MLP MAPE
K_e	0.9962	0.9966	2.90%
θ_p	0.9410	0.9264	5.34%
θ_{pc}	0.9666	0.9521	4.24%
M_y	0.9945	0.9929	2.38%
M_c	0.9954	0.9949	2.17%
Λ	0.9613	0.9439	5.83%

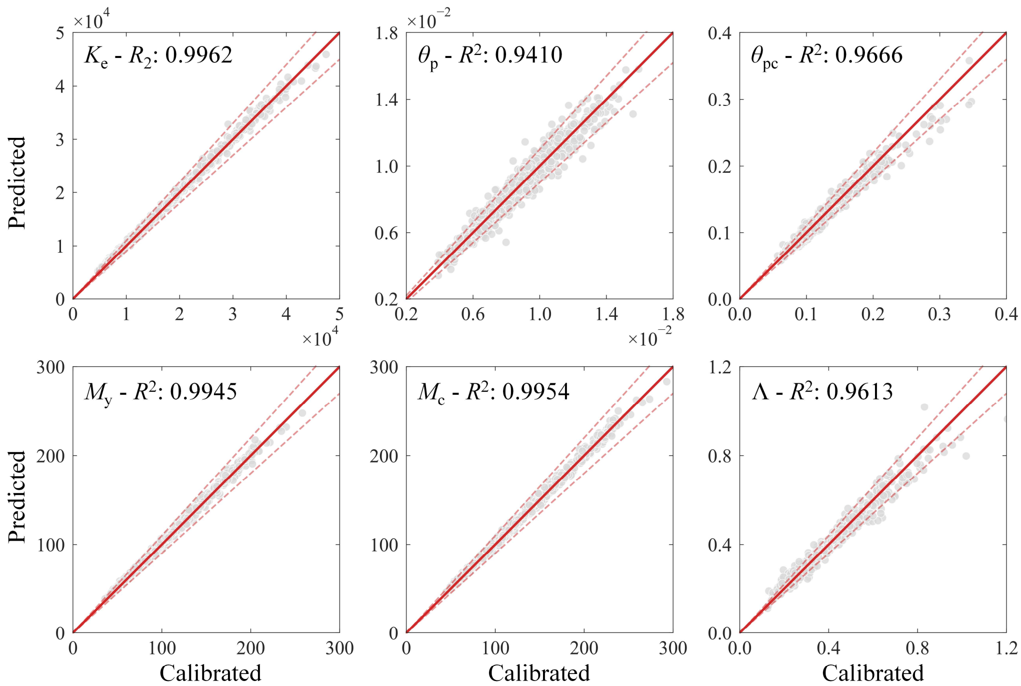

Figure 6. Comparison between the predicted and calibrated data

3.4 System-level integration

The system-level FE model was developed in OpenSees (Figure 7). The tower, blades, jacket members, and piles were represented using computationally cheaper beam elements. Following the well-established concentrated-plasticity approach, the HSTS was integrated into the system-level model using a coupled zero-length element assigned an mIMK uniaxial material whose parameters were provided by the MLP surrogate model, thereby forming an equivalent plastic-hinge representation.

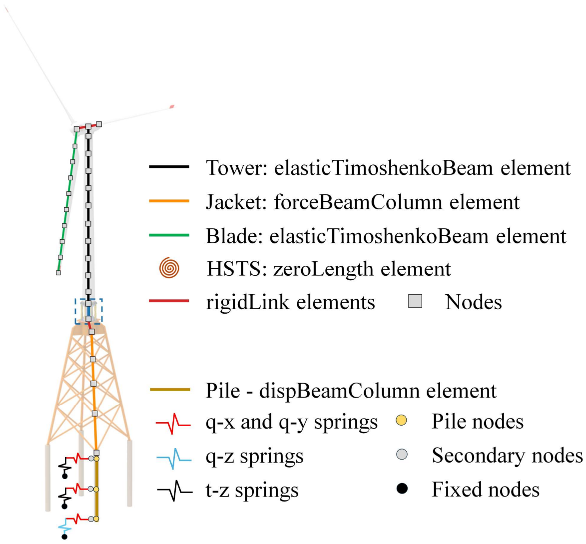

Figure 7. System-level FE model in OpenSees

4 Validation

4.1 Elastic structural dynamics

To validate the elastic structural dynamics of the developed surrogate-integrated FE model, a modal analysis was performed to obtain its periods of vibration in the fore-aft (FA) and side-side (SS) directions. Table 3 compares the periods of vibration of the FE model with the corresponding reference values for the prototype reported by von Borstel [20]. The differences are minor and the agreement is satisfactory, indicating that the proposed model captures the primary structural dynamics of the prototype with adequate fidelity.

Table 3. Periods of vibration of the surrogate-integrated FE model

Mode	Prototype (s)	FE model (s)
1st tower SS	3.49	3.52
1st tower FA	3.47	3.47
2nd tower SS	0.91	1.01
2nd tower FA	0.90	0.91

4.2 Hysteretic behaviour

The hysteretic response was finally reconstructed by feeding the predicted mIMK parameters and prescribed loading protocol into the HSTS FE model. Next, the reconstructed response was assessed against the corresponding FE-simulated response using the R^2 metric. Table 4 summarises the R^2 statistics over all 3000 samples, showing consistently accurate predictions with a mean R^2 value exceeding 0.96. In addition, approximately 3% of samples exhibit an R^2 below 0.90. Future research will prioritise the development of robust detection methods to ensure physical realism of hysteretic behaviour.

Table 4. Prediction performance of hysteretic behaviour

R^2	Train	Test	Overall
Mean	0.9649	0.9635	0.9646
Standard deviation	0.0284	0.0286	0.0284
Minimum	0.8538	0.8640	0.8539

4.3 Seismic behaviour

To validate the performance of the surrogate-integrated FE model regarding seismic assessment, a nonlinear time-history analysis (NLTHA) was conducted under the 1978 Tabas (Boshrooyeh) ground motion. Figure 8 compares tower-top displacements between the Abaqus model, comprising 19200 S4R and 1950 B31 elements, and the surrogate-integrated OpenSees model. The results demonstrate excellent agreement, with peak response discrepancies of around 8.6%.

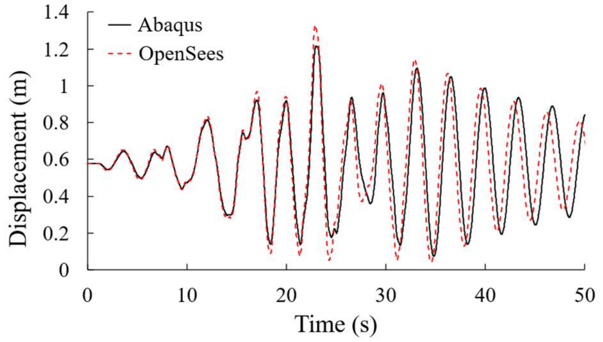

Figure 8. Seismic responses of the Abaqus model and the OpenSees model

Furthermore, to quantify efficiency gains, Table 5 summarises wall-clock times for representative analyses performed on an AMD Ryzen 9950X workstation. The surrogate model reduced hysteresis generation time from 16 minutes (Abaqus, 12-core configuration) to just 35 milliseconds. Moreover, the NLTHA was completed in 12.6 seconds via the OpenSees model, compared to 45 minutes for the Abaqus model, demonstrating its high computational efficiency for seismic assessment.

Table 5. Wall-clock times for representative analyses

Analysis	Abaqus	OpenSees
Hysteresis generation	16 min	35 ms
NLTHA	45 min	12.6 s

Overall, the proposed framework achieves a superior balance between predictive fidelity and computational efficiency. Beyond these performance gains, its modular architecture facilitates the integration of alternative ML algorithms, providing a versatile foundation for future comparative research into model performance.

5 Conclusions

This study presented a multi-fidelity surrogate-integrated modelling framework to enable efficient seismic assessment of tall energy infrastructures whose responses are governed by critical energy dissipation components.

The framework concentrates refined FE simulations on the critical component to generate a hysteresis database and trains a joint-prediction MLP surrogate to capture inter-parameter dependencies, thereby improving output consistency.

The approach was demonstrated on a representative 10-MW resilient JOWT, where an HSTS was characterised using a hysteresis database derived from 3,000 refined FE simulations and integrated into an OpenSees system-level model via a reduced-order plastic-hinge representation. The joint-prediction MLP model demonstrated consistently higher accuracy relative to independently trained XGBoost models – most notably for θ_p, θ_{pc}, and Λ. Validation results showed good agreement in modal properties and accurate hysteresis reconstruction (mean $R^2 > 0.96$), supporting the fidelity and efficiency of the proposed framework.

Acknowledgments

This work was financially supported by the National Key R&D Program of China (2025YFF0519700), the National Natural Science Foundation of China (Grant No. 52322802), the Zhejiang Provincial Natural Science Foundation (Grant No. LQN26E080033), and the Hangzhou Municipal Natural Science Foundation (Grant No. 2025SZRJJ1193).

References

[1] GWEC. Global Wind Report 2025. The Global Wind Energy Council, Lisbon, Portugal, 2025.

[2] B. Hernández, N. L. Ferber, M. Abdullah, A. Mayyas, N. Calvet, and M. Chiesa, Central receiver-based concentrated solar power plants part 1: A historical review, *Sol. Energy* 299(2025) 113693.

[3] E. I. Katsanos, S. Thöns, and C. T. Georgakis, Wind turbines and seismic hazard: a state-of-the-art review, *Wind Energy* 19(2016) 2113–2133.

[4] N. Alati, G. Failla, and F. Arena, Seismic analysis of offshore wind turbines on bottom-fixed support structures, *Phil. Trans. R. Soc. A.* 373(2015) 20140086.

[5] H. Zuo, K. Bi, and H. Hao, Using multiple tuned mass dampers to control offshore wind turbine vibrations under multiple hazards, *Eng. Struct.* 141(2017) 303–315.

[6] M. Liu, S. Li, T. Wu, Y. Li, H. Meng, and Z. Chen, Eddy-Current Tuned Mass Dampers for Mitigation of Wind-Induced Response of the Noor III Solar Tower: Design, Installation, and Validation, *J. Struct. Eng.* 147(2021) 05021009.

[7] A. Hemmati, E. Oterkus, and N. Barltrop, Fragility reduction of offshore wind turbines using tuned liquid column dampers, *Soil Dyn. Earthquake Eng.* 125(2019) 105705.

[8] Y. Li, S. Li, B. Sun, M. Liu, and Z. Chen, Effectiveness of a tiny tuned liquid damper on mitigating wind-induced responses of cylindrical solar tower based on elastic wind tunnel tests, *J. Wind Eng. Ind. Aerodyn.* 208(2021) 104455.

[9] R. Rostami and A. Tombari, A novel reduced column section approach for the seismic protection of wind turbines, *Eng. Struct.* 282(2023) 115807.

[10] K. Ke, W. Xie, X. Zhou, Y. Wang, and X. He, A novel self-centring jacket-type offshore wind turbine structure: A proof-of-concept study and seismic fragility analysis, *Thin-Walled Struct.* 205(2024) 112407.

[11] T. Wang et al., From model-driven to data-driven: A review of hysteresis modeling in structural and mechanical systems, *Mech. Syst. Signal Process.* 204(2023) 110785.

[12] S. Chen, D. Feng, and E. Taciroglu, Prior knowledge - infused neural network for efficient performance assessment of structures through few - shot incremental learning, *Computer aided Civil Eng.* 39(2024) 1928–1945.

[13] Y. Yan, Y. Yang, M. Bashir, C. Li, and J. Wang, Dynamic analysis of 10 MW offshore wind turbines with different support structures subjected to earthquake loadings, *Renew. Energy* 193(2022) 758–777

[14] D. Samadian, I. B. Muhit, A. Occhipinti, and N. Dawood, Surrogate models for seismic and pushover response prediction of steel special moment resisting frames, *Eng. Struct.* 314(2024) 118307.

[15] G. Georgiou and A. Elkady, ANN-Based Model for Predicting the Nonlinear Response of Flush Endplate Connections, *J. Struct. Eng.* 150(2024) 04024034.
[16] C.-L. Ning, L. Wang, and W. Du, A practical approach to predict the hysteresis loop of reinforced concrete columns failing in different modes, *Constr. Build. Mater.* 218(2019) 644–656.
[17] T. A. Horton, I. Hajirasouliha, B. Davison, and Z. Ozdemir, Accurate prediction of cyclic hysteresis behaviour of RBS connections using Deep Learning Neural Networks, *Eng. Struct.* 247(2021) 113156.
[18] W. Xie, X. Zhou, K. Ke, M. C. H. Yam, and Y. Yan, A resilient jacket-type offshore wind turbine system: Conception, surrogate-integrated modelling, and seismic performance evaluation, *Ocean Eng.* 349(2026) 124123.
[19] D. G. Lignos and H. Krawinkler, Deterioration Modeling of Steel Components in Support of Collapse Prediction of Steel Moment Frames under Earthquake Loading, *J. Struct. Eng.* 137(2011) 1291–1302.
[20] T. von Borstel, Design Report Reference Jacket (No. D4.3.1). INNWIND.EU, 2013.